I&EC research
Industrial & Engineering Chemistry Research

pubs.acs.org/IECR

Article

Robust, Small Diameter Hydrophilic Nanofibers Improve the Flux of Ultrafiltration Membranes

Kerianne M. Dobosz, Christopher A. Kuo-Leblanc, Jared W. Bowden, and Jessica D. Schiffman*

Cite This: https://doi.org/10.1021/acs.iecr.1c01332

Read Online

ACCESS | Metrics & More | Article Recommendations | Supporting Information

ABSTRACT: In this study, we systematically investigated the flux performance of ultrafiltration (UF) membranes functionalized with randomly accumulated nanofibers. By electrospinning nanofibers from hydrophobic polysulfone (PSf) and hydrophilic cellulose (CL), we were able to explore the role that the bulk nanofiber (NF) layer thickness, individual NF diameter, and intrinsic chemistry play in composite membrane flux. Additional parameters that we systematically tested include the molecular weight cut-off (MWCO) of the base membrane (10, 100, and 200 kDa), flow orientation (cross-flow versus dead-end), and the feed solution (hydrophilic water versus hydrophobic oil). Structurally, the crosslinked PSf nanofibers were more robust than the CL nanofibers, which lead to the PSfNF-UF membranes having a greater flux performance. To decouple the structural robustness from the water affinity of the fibers, we chemically modified the PSf fibers to be hydrophilic and, indeed, the flux of these new composite membranes featuring hydrophilic crosslinked nanofibers was superior. In summary, the greatest increase in flux performance arises from the smallest diameter, hydrophilic nanofibers that are mechanically robust (crosslinked). We have demonstrated that electrospun nanofibers improve the flux performance of ultrafiltration membranes.

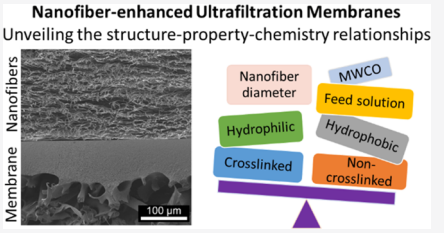

INTRODUCTION

Diarrhea is the second leading cause of death for children under the age of five, leading to 2195 deaths every day. Approximately 88% of these deaths are attributed to unsafe water, inadequate sanitation, and insufficient hygiene.[1,2] Membrane-based technologies offer an effective approach to providing clean drinking water by removing the harmful bacteria associated with childhood mortality. Specifically, pressure-driven ultrafiltration membranes can eliminate the risks of microorganisms (i.e., a 6.9 log reduction of *Escherichia coli*) without the use of chlorine.[3,4] Further advantages of ultrafiltration membranes include their high water production, i.e., 50 to 200 gallons per square foot of membrane per day, and their low energy requirement because they operate at low pressures, i.e., 3.4 bar (50 psi).[5] Unfortunately, during water production, undesirable contaminants accumulate on the surface of the membranes in a process known as fouling. Fouling reduces membrane flux performance and, over time, requires the operation to shut down for cleaning. Thus, the associated costs of membrane-based separation increases; research into improving the antifouling properties of ultrafiltration membranes is needed to extend their operating lifetime.

A vast number of efforts to improve the fouling resistance of membranes have focused on functionalizing the membrane's surface with antifouling and/or antibacterial agents, such as hydrophilic polymers or biocidal agents.[6,7] However, there are detrimental effects that result from these surface modifications, including membrane flux decline and/or deviation from the designed membrane selectivity. In addition to chemical agents, geometry has been explored by patterning the surface of membranes with stripes, pillars, and/or prisms.[8] Unique surface morphology successfully reduces fouling by particles and/or bacteria, but the fabrication methods used, such as nanoimprint lithography and non-solvent-induced patterning, have distorted the membrane pores, have reduced membrane integrity, and are often challenging to scale to commercial production.[9−18] An alternative approach, which has been suggested by our group, as well as by others, is to apply a scalable, high porosity fibrous layer to the surface of the membrane that can improve membrane performance without altering base membrane properties.[19−21]

Electrospinning can be used to manufacture textiles on the commercial scale that are comprised of randomly accumulated nanofibers with large surface-to-volume ratios, high specific surface areas, large interstitial spaces, and porosity values greater than 80%.[22,23] Nanofibers show promise in a wide range of separation applications, including membrane distillation, adsorption, pretreatment of feed, and reverse osmosis membranes.[24−27] Models have suggested that the performance of freestanding nanofiber mats with small fiber diameters of ∼2 and ∼70 nm with membrane thicknesses of <100 and <1000

Received: April 7, 2021
Revised: June 4, 2021
Accepted: June 8, 2021

nm, respectively, would surpass that of current ultrafiltration and microfiltration membranes.[28] When Liu *et al.*[19] deposited a ~5 μm-thick layer of carbon nanofibers (diameter: 20−40 nm) onto ultrafiltration membranes, they demonstrated a minimal pure water flux decline and an improved removal of natural organic matter, including sodium alginate and bovine serum albumin. A layer of poly(acrylic acid) and poly(vinyl alcohol) nanofibers (<2 mg/cm^2) was electrospun onto ultrafiltration membranes, causing an increase in membrane hydrophilicity and a reduction in organic fouling without affecting permeability or protein rejection performance.[21] Previously, we investigated the effect of altering the surface of ultrafiltration membranes with a 50 μm-thick cellulose (CL) or polysulfone (PSf) electrospun layer that consisted of randomly accumulated 1.0 μm-diameter fibers.[20] Fouling resistance was improved and selectivity was retained by ultrafiltration membranes that were enhanced using a nanofiber layer. Potentially, due to their better mechanical integrity, the PSf nanofiber membranes demonstrated a higher pure water permeance across a greater range of transmembrane pressures than the CL nanofiber membranes or the control membranes (no nanofibers). Despite the promising preliminary results acquired across different laboratories, the literature is currently lacking a systematic study that fundamentally probes the chemistry−structure−property relationships that govern nanofiber-enhanced membrane performance.

Here, we systematically investigated the performance of nanofiber-enhanced membranes. Parameters we investigated, which had not yet been tested, include the molecular weight cut-off of the base ultrafiltration membrane, electrospun nanofiber characteristics (i.e., chemistry, bulk thickness, hydrophilicity, and nanofiber diameter), pure water flow orientation (cross-flow versus dead-end), and feed solution hydrophobicity (hydrophilic water versus hydrophobic oil). Expanding our understanding of the chemistry−structure−property relationships of composite nanofiber ultrafiltration membranes hold potential to enable the *a priori* design of membranes with improved flux and antifouling performance to be used across a wide variety of separation applications.

MATERIALS AND METHODS

Materials and Chemicals. All compounds were used as received. Polysulfone (PSf; Mn: 22,000 Da), cellulose acetate (M_n = 30,000 Da), *N*,*N*-dimethylformamide (DMF; anhydrous, 99.8%), tetrahydrofuran (THF; 250 ppm BHT as an inhibitor, ACS reagent, ≥99.0%), 2-propanol, and dopamine hydrochloride (dopamine) were obtained from Sigma-Aldrich (St. Louis, MO). Acetone (histological grade), ethanol (absolute anhydrous, 200 Proof), sodium hydroxide (NaOH), and tris-(hydroxymethyl)aminomethane (tris) were purchased from Fisher Scientific (Pittsburgh, PA). Polydimethylsiloxane silicone oil (1 cst) was purchased from Clearco Products (Willow Grove, PA). Deionized (DI) water was obtained from a Barnstead Nanopure Infinity water purification system (Thermo Fisher Scientific, Waltham, MA).

Electrospinning of CL, PSf, and Hydrophilic Nanofibers. The procedure used to electrospin CL was based on the literature.[20,29] The electrospinning precursor solution (15 w/v cellulose acetate in acetone) was mixed for 24 h using an Arma-Rotator A-1 (20 rpm, Elmeco Engineering, Rockville, MD). The polymer solution was loaded into a 5 mL Luer-Lock tip syringe capped with a Precision Glide 18-gauge needle (Becton, Dickinson & Company, Franklin Lakes, NJ) before being secured to an infusion syringe pump (Cole Parmer, Vernon Hills, IL). Alligator clips were used to connect the electrode of a high-voltage supply (Gamma High Voltage Research, Ormond Beach, FL) to the needle and to the collection plate, which was a copper plate wrapped in aluminum foil (152.4 mm × 152.4 mm × 3.175 mm, McMaster-Carr, Robbinsville, NJ) held at a 10 cm fixed separation distance. A constant feed rate of 3 mL/h with an applied voltage of 25 kV was used. The electrospinning apparatus was housed in a custom-built environmental chamber equipped with a desiccant unit (Drierite, Xenia, OH) maintained at 22 ± 1 °C with a relative humidity of 55%. Cellulose acetate solutions were electrospun for 1.0 h to generate layers with a consistent bulk thickness (*z*-axis), which was confirmed by averaging 25 different measurements on 5 separate samples using a Mitutoyo 293-330 digital micrometer (Ontario, Canada). The bulk nanofiber layers were sandwiched between Teflon sheets (3.2 mm × 101.6 mm × 152.4 mm, McMaster-Carr) and placed in an oven for 1 h at 208 °C. To regenerate the cellulose acetate nanofibers into cellulose (CL) nanofibers, the heat-treated nanofibers were submerged into a 0.1 M sodium hydroxide solution (4/1 v/v of DI water/ethanol) for 14 h before being washed three times with DI water.

PSf nanofibers were fabricated using the same electrospinning apparatus. The precursor solutions used to electrospin small, medium, and large diameter PSf nanofibers were comprised of 18, 21, and 25 wt % PSf in THF/DMF (1/1 w/w), respectively. A 5 mL Luer-Lock tip syringe was capped with a blunt-tipped 22-gauge needle and constant feed rates of 2.0, 1.8, and 1.8 mL/h were used. All PSf solutions were electrospun using an applied voltage of 17 kV for 0.33 h at 23% relative humidity. As-spun nanofibers were heat-treated at 165 °C for 1 h between Teflon sheets.

Hydrophilic PSf nanofibers were synthesized by functionalizing as-spun PSf nanofibers with a polydopamine coating based on the literature.[8,30] The as-spun nanofibers were submerged in 2-propanol for 0.5 h and then DI water for 0.5 h before being loaded into a reaction chamber (38 mm diameter) that was loaded with a solution of 75 mL of tris and 1.5 g of dopamine. The system was agitated at 150 rpm for 1 h. Upon removing the functionalized nanofibers, they were submerged in ethanol for 0.17 h, rinsed three times with DI water, and soaked for 1 h in DI water before being rinsed three times with DI water to remove any non-reacted or non-adhered dopamine. All nanofiber layers were stored dry at 23 °C and acclimated to room temperature (23 ± 1 °C) by submerging them in DI water for 0.33 h prior to use.

Assembly of Nanofiber-Enhanced Ultrafiltration Membranes. Polyethersulfone membranes from EMD Millipore (Burlington, MA) and Synder Filtration Inc. (Vacaville, CA) with reported molecular weight cut-offs (MWCOs) of 10, 100, and 200 kDa were used as the base membranes. Nanofiber layers were synthesized in-house as described in the previous section.

To create a nanofiber-enhanced ultrafiltration membrane, the in-house fabricated nanofiber layer was placed on the surface of the commercial membrane.[20] The bonding strength between the membrane and the nanofiber layer was not enhanced; no heat treatment or adhesives were applied. The thickness of the assembled composite membrane was determined by taking measurements at 25 different locations on 5 separate samples using a Mitutoyo 293-330 digital

https://doi.org/10.1021/acs.iecr.1c01332
Ind. Eng. Chem. Res. XXXX, XXX, XXX−XXX

micrometer. Internal O-rings in the testing cells held the composite membrane in place throughout testing. Throughout Results and Discussion of this paper, the control membranes without nanofibers will be referred to as UF# and composite membranes with a CL or a PSf nanofiber layer will be referred to as CLNF-UF# or PSfNF-UF#, respectively, where the # refers to the MWCO of the base membrane (10, 100, or 200 kDa).

Materials Characterization. Nanofiber chemistry was confirmed using Fourier transform infrared spectroscopy (FTIR, Bruker Alpha, Bruker Optics, Billerica, MA). Contact angle measurements using 4 μL drops of DI water were carried out using a home-built apparatus equipped with a Nikon D5100 digital camera with a 60 mm lens and 68 mm extension tube (Melville, NY).[31] The contact angle reported is the average of 25 drops on 5 different nanofiber layers and membranes. Micrographs of membrane cross sections were acquired using an EVO50 scanning electron microscope (Carl Zeiss Inc., Thornwood, NY). Cross-sectional scanning electron microscopy (SEM) micrographs were obtained after removing the fabric support layer from the commercial ultrafiltration membrane, submerging the sample in liquid nitrogen, and cracking the sample.[32] Samples were coated with a xenon magnetron sputter XE200 (Edwards Vacuum, Albany, NY) for 30 s. Nanofiber diameter distribution was determined using ImageJ 1.47 (National Institutes of Health, Bethesda, MD) by measuring 50 random fibers from 5 micrographs.[33] Higher-resolution micrographs of membrane pores were acquired using a Magellan 400 XHR scanning electron microscope (FEI, Hillsboro, OR). Membranes were sputter-coated for 40 s with platinum before SEM imaging (Cressington 208 HR, Cressington Scientific Instruments, Watford, England). Using ImageJ, a total of 100 pore measurements from 5 separate membrane samples were taken to determine the average membrane pore diameter. Pore coverage was determined using ImageJ threshold and particle analysis functions.

Cross-Flow Performance of Nanofiber-Ultrafiltration Membranes. Prior to use, all membranes were flushed using a custom-built cross-flow cell (28 mm long, 17 mm wide, and 1.5 mm deep, with an active area of 5.44 cm^2) equipped with a 31 mil (0.7874 mm) low foulant spacer and a permeate carrier (Sterlitech Corporation, Kent, WA), consistent with our previous study.[20] All tests were conducted at a flow rate of 50 mL/min enabled by a reciprocating pump (Eldex Laboratories Incorporated, Napa, CA) followed by a dampener (Cat Pumps, Minneapolis, MN).[34−36] Two distinct flushing procedures were used on the two commercial membranes following industry recommendations. To flush the Millipore membranes (29 mm × 45 mm), they were placed active side down in the cross-flow cell and flushed with DI water at a transmembrane pressure (TMP) of 1.5 bar (21.8 psi), where the TMP was held for 0.016 h to remove glycerol (a preservation substance) as confirmed by high-performance liquid chromatography (HPLC). The Synder membranes were flushed at a TMP of 4.1 bar (60 psi) for 0.083 h. Flushed membranes were either used immediately or stored in DI water at 4 °C. If stored, the membranes in DI water were reacclimated to 23 °C by submerging them for 0.33 h into room-temperature DI water prior to their use.

To test nanofiber-enhanced membranes, the cross-flow cell was disassembled and a pre-wet CL or PSf nanofiber layer (29 mm × 45 mm × 0.051 mm) was placed below the flushed and compacted membrane before reassembling the flow cell and applying the desired TMP. The pre-wetting procedure consisted of submerging the nanofiber layer in room-temperature (23 ± 1 °C) DI water for 12 h prior to use. An example compaction curve (Figure S1) displays that the change in flux was less than 5% after 0.17 and 1 h for the Synder and Millipore membranes, respectively. Thus, we report cross-flow flux values after 0.17 and 1 h for the compacted Synder and Millipore membranes, respectively. Membrane permeability, or the increase in membrane throughput as a function of increase in TMP, was determined using eq 1:[37]

$$\text{hydraulic permeance}\left(\frac{\text{L}}{\text{m}^2\ \text{h bar}}\right) = \frac{\text{pure water flux}}{\text{TMP}} \quad (1)$$

with the compacted flux data for TMPs ranging from 0.5 to 3.5 bar. Experiments were conducted in triplicate.

To calculate the membrane surface area that was blocked by the spacer during cross-flow operation, the spacer was pressed onto a gel-based stamp pad (Costco Wholesale, Seattle, WA) and installed in the cross-flow cell. The membrane was placed active side down onto the O-ring and a 1.5 kg mass was placed on top of the support layer of the membrane. The particle analysis function in ImageJ was used to calculate the membrane's surface coverage based on digital images acquired from five replicates.

Dead-End Performance of Nanofiber-Ultrafiltration Membranes. A dead-end stirred cell (Sterlitech) equipped with an acrylic ring (22 mm inner diameter) created a membrane active area of 201 mm^2.[38,39] First, the preservative materials were flushed from the membrane pores by following an industry-recommended protocol. To flush Millipore membranes (102 mm-diameter circles), they were immersed in 2-propanol for 0.5 h, rinsed three times with DI water, immersed in DI water for 0.5 h, and then rinsed three times with DI water.[20] Synder membranes were flushed over 0.083 h using 2 L of DI water at an applied pressure of 4.1 bar (60 psi) without stirring. Flushed nanofiber-enhanced membranes (25 mm circles) were loaded into the disassembled dead-end stirred cell after being pre-wet (submerged in DI water for 12 h). The nanofiber layers had a bulk thickness that ranged from 25 to 125 μm and an average fiber diameter ranging from 0.4 to 1.7 μm. The dead-end stirred cell was reassembled with the acrylic ring and O-ring before TMP (0.5, 1.0, and 3.5 bar) was applied. The TMP for dead-end operation was calculated as the inlet pressure minus the permeate pressure. The pure water permeate was collected in a beaker placed on a balance connected to Serial Port Monitor (Eltima, Frankfurt, Germany) to record mass versus time for 0.25 or 1.0 h for the Synder and Millipore membranes, respectively, to be consistent with the cross-flow procedure.

To characterize the hydrophobic flux performance of the membranes, oil flux tests were conducted. The Millipore UF100 were flushed by immersing them in 2-propanol for 0.5 h, DI water for 0.5 h, 2-propanol for 0.5 h, and then silicone oil for 0.5 h. Using the same experimental setup, 200 mL of silicone oil was loaded into the pressure vessel and the permeate was collected in a beaker for 0.25 h at 0.016 h increments at TMPs of 2 and 3.5 bar.

Statistics. Throughout Results and Discussion, the statistical differences between samples were determined using an unpaired Student's *t*-test with a *p*-value of 0.05.

https://doi.org/10.1021/acs.iecr.1c01332
Ind. Eng. Chem. Res. XXXX, XXX, XXX−XXX

RESULTS AND DISCUSSION

Characteristics of CL and PSf Nanofibers and Nanofiber-Enhanced Membranes. We successfully electrospun cellulose (CL) and polysulfone (PSf) nanofibers with an equivalent average fiber diameter and bulk thickness. CL was chosen as the hydrophilic polymer because it is the most abundant natural polymer and is commonly used in environmental applications. Hydrophobic nanofibers were electrospun from PSf, another polymer used frequently in membrane applications. The CL nanofibers had a smooth continuous morphology with an average diameter of 1.0 ± 0.5 μm (Figure 1). As evident from the micrographs, the fibers have a

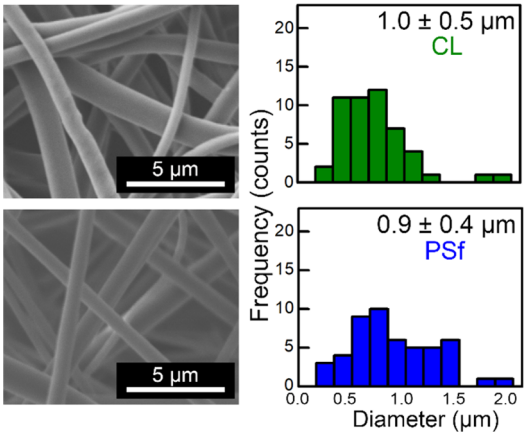

Figure 1. SEM micrographs of the electrospun (top) CL and (bottom) PSf nanofibers along with their average fiber diameter and diameter distribution.

cylindrical morphology and their surfaces do not show any signs of roughness (i.e., bumps or dimples). Additionally, no fiber ends or short fibers were observed in any of our acquired micrographs. Fourier-transform infrared spectroscopy (FTIR) (see Figure S2) was used to confirm that the electrospun cellulose acetate nanofibers were successfully converted to cellulose via an alkaline treatment. The disappearance of the 1750 cm^{-1} peak indicates that the acetate groups have been replaced with hydroxyl groups. Contact angle measurements confirmed that the CL nanofibers exhibited a hydrophilic water contact angle of 0°, consistent with the literature.[29,40,41] Additionally, PSf nanofibers electrospun from a 21 wt % PSf precursor solution created fibers with an average diameter of 0.9 ± 0.4 μm, which is statistically equivalent to the CL nanofibers. FTIR confirmed their PSf chemistry, and their hydrophobicity was confirmed via their 112 ± 5° water contact angle.[42,43] These same diameter CL and PSf nanofibers were next used to investigate the influence of structure−property−chemistry relationships on the flux performance of composite ultrafiltration membranes.

A layering technique was used to assemble the composite membranes (Figure 2). The representative images display that the base ultrafiltration (UF) membranes had a sponge-like morphology (Figure 2, left),[44] whereas the added nanofiber layer was highly porous and fibrous. We present these cross-sectional images to help the reader see the difference in the structure between the enormous porosity offered by the nanofiber mat and the commercial membrane. The air gap between the PSf nanofiber layer and the membrane (Figure 2, right) is an artifact of sample preparation that commonly

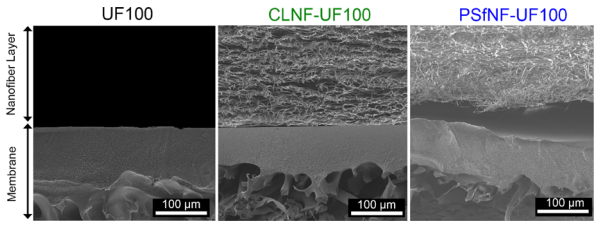

Figure 2. Representative cross-sectional SEM micrographs of control UF100, CLNF-UF100, and PSfNF-UF100 membranes. The CL and PSf nanofiber layers have a bulk thickness of 50 μm and an average individual fiber diameter of 1.0 μm. Millipore membranes were used as the base.

occurs due to liquid nitrogen cracking and SEM imaging that involves sample drying and applying vaccum.[45] Composite membranes used in our studies were well wet (see Materials and Methods) and showed no signs of delamination. Additionally, the bulk thickness in the micrographs appears larger than what we carefully confirmed using a digital micrometer.

Dead-End Pure Water Flux of CLNF-UF and PSfNF-UF Membranes as a Function of Bulk Nanofiber Layer Thickness. We first focused on determining the optimal nanofiber layer thickness to use in further experiments by examining the statistical correlation between pure water flux and nanofiber bulk thicknesses (i.e., 25, 50, 75, 100, and 125 μm). All composite membranes were tested using a TMP of 2 bar in dead-end configuration (Figure 3). As the bulk thickness

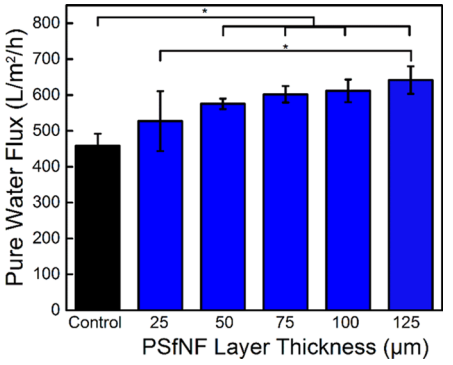

Figure 3. Dead-end flux of PSfNF-UF100 membranes as a function of bulk layer thickness. All nanofiber layers were composed of individual fibers with 1 μm diameters. Synder membranes were used as the base. An operating pressure of 2 bar was used. The error bars indicate standard deviation, and one asterisk (*) denotes $p < 0.05$ significance.

increased from 50 μm to 125 μm, the flux increased from 527 ± 15 $L/m^2/h$ to 641 ± 40 $L/m^2/h$, respectively. Both flux values are statistically greater than the control UF100 membrane. Additionally, the pure water flux of the PSfNF-UF100 membranes with the thickest layer (125 μm) was statistically greater than the composite membrane featuring a 50 μm-thick layer, thereby suggesting that this set of experiments has yet to find the upper limit where the bulk nanofiber thickness decreases the flux using this setup. While the flux of the 25 μm PSfNF-UF100 was trending to a higher value than the control membrane, it was not statistically greater. This suggests that a lower limit or minimum thickness of the fibrous layer is required to induce improved fluid dynamics.

https://doi.org/10.1021/acs.iecr.1c01332
Ind. Eng. Chem. Res. XXXX, XXX, XXX−XXX

Table 1. Properties of the Base Ultrafiltration Synder Membranes with Various MWCOs

Synder membrane (sample name)	MWCO (kDa)	pore diameter (nm)	pore coverage (%)	contact angle (°)	thickness (μm)
UF10	10	0.52 ± 0.2	5 ± 0.3	59 ± 6	175 ± 8
UF100	100	1.15 ± 0.1	11 ± 0.3	61 ± 5	200 ± 15
UF200	200	1.50 ± 0.1	12 ± 0.3	62 ± 6	210 ± 5

Experiments were also conducted using CL nanofiber layers with bulk thicknesses of 20, 50, 65, and 125 μm (Figure S3). The UF membranes featuring a 50 μm- or 65 μm-thick CL nanofiber layer both exhibited a statistically greater flux than the control (no nanofibers) and the thickest layer of nanofibers (125 μm). Notably, this trend, where thinner CL layers (50 and 65 μm) showed improved flux over the thickest nanofibers, opposes that observed for the PSfNF composite membranes. We suggest that the CL nanofiber's hydrophilic and non-crosslinked chemistry is causing them to swell and physically move, which is why we do not observe further flux enhancement, consistent with what has been reported in more traditional membrane modifications.[46] Additionally, the CL nanofiber layers that were 20 μm thick did not withstand the testing at a TMP of 3.5 bar, emphasizing their lower mechanical integrity[47] in comparison to the PSf nanofibers, which do withstand the same testing. Based on these results, our next experiments utilized the 50 μm-thick CL and PSf nanofibers as these show excellent flux results and were experimentally parallel.

Cross-Flow Pure Water Flux of CLNF-UF and PSfNF-UF Membranes as a Function of MWCO. We next determined the effect that the 50 μm-thick CL and PSf nanofibers had on three commercial Synder membranes with varying MWCOs. Table 1 displays that, as expected, the average pore diameter and pore coverage (i.e., pore area per membrane area) had a positive correlation with MWCO. Additionally, the UF membranes all had a statistically equivalent contact angle.

The cross-flow pure water flux of the UF10, UF100, and UF200 membranes enhanced with a 50 μm-thick nanofiber layer that was comprised of 1 μm-diameter fibers is displayed in Figure 4 and Figure S4. At a TMP of 2 bar, all PSfNF-UF membranes exhibited a statistically greater flux than the controls (no nanofibers). A PSf nanofiber layer on the UF10, UF100, and UF200 membranes exhibited 25, 15, and 20% increases in flux versus their control membrane (no nanofibers), respectively. The observed flux increases are statistically equivalent, suggesting that the 50 μm-thick PSf nanofiber layer had an equivalent effect regardless of the base membrane selectivity.

On the other hand, all CL nanofiber-enhanced membranes exhibited a flux that was equivalent to that of the control. The UF10 exhibited a cross-flow pure water flux of 64 ± 2 L/m^2/h compared to 61 ± 4 L/m^2/h for the CLNF-UF10. A flux of 285 ± 41 L/m^2/h was observed for the control UF100 versus 260 ± 23 L/m^2/h for the CLNF-UF100. Additionally, a flux of 591 ± 84 L/m^2/h versus 672 ± 18 L/m^2/h was determined for the control and CLNF-UF200, respectively. Our results for the CL nanofibers are similar to those observed when other hydrophilic electrospun fibers were loaded onto membranes; the polymeric fiber layer did not significantly add hydraulic resistance or have a negative effect on the water flux performance.[21] Our previous results demonstrated that the nanofiber layer has no effect on the MWCO value; the nanofiber-enhanced membranes had the same MWCO as the control membrane (no nanofibers).[20] These results demonstrate that by adding a highly porous swellable fiber layer to an ultrafiltration base membrane, we retain high flux values but do not see the same flux increase that is observed with the PSf fibers. This is a notable result as, typically, the addition of nanomaterials to the surface of a membrane decreases its flux.

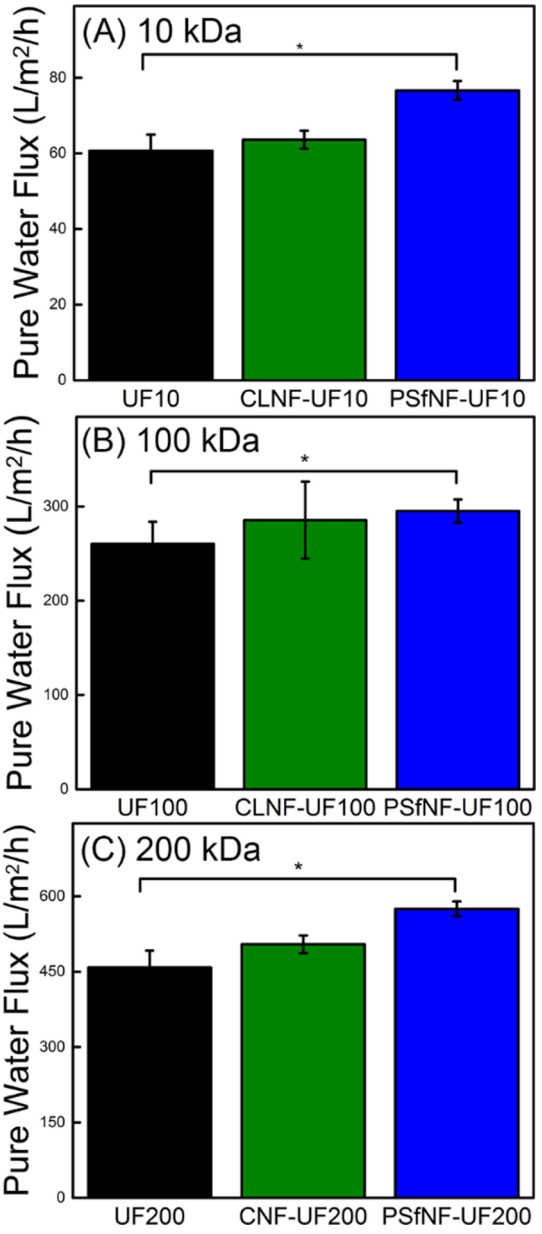

Figure 4. Cross-flow pure water flux performance of CLNF-, PSfNF-, and control (A) UF10, (B) UF100, and (C) UF200 membranes. All nanofiber layers were 50 μm thick and had an average individual fiber diameter of 1.0 μm. Data was collected at a TMP of 2 bar. Synder membranes were used as the base. The error bars indicate standard deviation, and one asterisk (*) denotes $p < 0.05$ significance. Figure S4 provides an alternative display of the same data.

https://doi.org/10.1021/acs.iecr.1c01332
Ind. Eng. Chem. Res. XXXX, XXX, XXX−XXX

During cross-flow testing, a spacer sits on the surface of the membrane, covering some amount of the membrane surface and pores. We experimentally determined that our spacer covers 3.5 ± 0.8% of the base membrane's surface (Figure S5). In the case of our composite membranes, the spacer sits on top of the nanofiber layer and does not directly contact or block the membrane pores. Notably, due to their random fiber orientation, our non-woven mats have a minimal flat surface that would be in direct contact with the membrane's surface. In fact, it was not possible to capture representative ink blots of the nanofiber-enhanced membrane's surface analogous to what we have displayed in Figure S5 using the bare membrane.

All three PSfNF-enhanced membranes, regardless of the base MWCO, demonstrated a flux increase of ∼20%. Normalizing the increase in membrane flux by the pore coverage for the three membranes demonstrated that the membrane with the smallest MWCO value exhibited the greatest improvement. We found that the PSfNF-UF10 membranes, which had the smallest pore diameter and coverage, exhibited a 50% increase in normalized flux, whereas the PSfNF-UF100 and PSfNF-UF200 membranes exhibited 11 and 14% improvement over their controls. The increase in flux exhibited by the PSfNF-UF10 membranes was statistically greater than the PSfNF-UF100 and PSfNF-UF200 membranes. We hypothesize that this result is at least partially due to the crosslinked PSf fibers acting like a spacer to increase local turbulence in cross-flow configuration.[20,48] We can support this hypothesis via the CLNF membrane's statistically equivalent flux. As previously discussed, the non-crosslinked CL fibers swell in the presence of water[46] and are less robust than the PSf fibers. To decouple the effect of chemistry from the effect of mechanics, the performance of a non-swellable, crosslinked hydrophilic nanofiber layer was also tested and will be discussed later (see Figure 6).

Dead-End Pure Water Flux of CLNF-UF and PSfNF-UF Membranes as a Function of MWCO. We next used a dead-end flow cell, where the bulk feed approaches perpendicular to the membrane surface, to investigate if a nanofiber layer would impact the pure water flux of membranes with different MWCOs. Typically, dead-end operation is conducted with agitation to reduce concentration polarization. As this mixing creates artificial local fluid conditions that are cross-flow-like, we conducted our tests without agitation to best probe the effect of feed geometry. However, as shown in Figure S6, there was no statistical difference in flux most likely due to the fact there was no solute in these experiments. At the lowest TMP (0.5 bar), the UF100 membranes with and without a 50 μm-thick CL or PSf nanofiber layer exhibited a statistically equivalent flux of ∼350 L/m^2/h (Figure 5). Increasing the operating pressure revealed a strong dependence between nanofiber layer chemistry (CL versus PSf) and membrane flux behavior. At a TMP of 1.0 bar, the CLNF-UF composite membranes exhibited a statistically equivalent flux to the base membranes; however, at 3.5 bar, the CL composite membranes exhibited a 51% decrease in dead-end flux. On the other hand, there was a positive correlation between TMP and pure water flux for the PSfNF-UF100, and the pure water flux increased by 20 and 65% over the controls at 1 and 3.5 bar, respectively.

Once again, the PSf nanofibers showed improved performance over the CL and controls, especially at higher TMPs. While the PSf nanofibers have a higher tensile strength and are crosslinked, which greatly aid in promoting flux increases,[49,50]

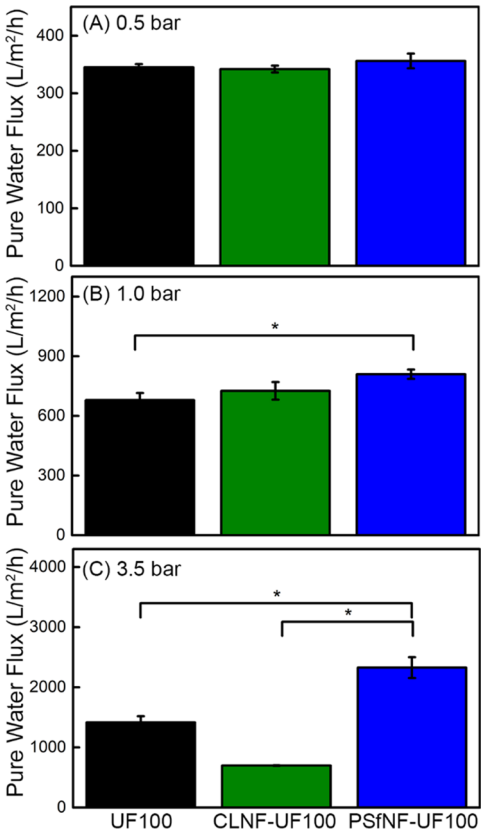

Figure 5. Dead-end pure water flux of control, CLNF-, and PSfNF-UF100 membranes as a function of TMP: (A) 0.5 bar, (B) 1.0 bar, and (C) 3.5 bar. All nanofiber layers were 50 μm thick with an average fiber diameter of 1 μm. Synder membranes were used as the base. The error bars indicate standard deviation, and one asterisk (*) denotes $p < 0.05$ significance.

the CL fibers are more likely to vibrate or physically move at higher TMPs, therefore disrupting their orientation.[21,51−53] Notably, all nanofibers were durable as we never observed any broken fibers post testing (SEM micrographs not shown). Our results are supported by a previous report from Shou *et al.*[50] who demonstrated that randomly packed fibrous media have a larger permeability than regularly organized media and that hydraulic permeability increases with an increasing degree of randomness.

Typically, when two layers are in series, they both increase the overall resistance. However, in our case, the interstitial spacing between fibers is large (∼3 μm) and the permeance of the nanofiber layer is 3 orders of magnitude greater than the selective membranes, as we have previously investigated.[30] Therefore, the resistance of the nanofiber layer is negligible. We calculated that the UF100 membranes had a hydraulic permeance of 410 L/m^2/h/bar, whereas the same membranes with a 50 μm-thick nanofiber layer of PSf nanofibers had a hydraulic permeance of 800 L/m^2/h/bar at operating pressures from 0.25 to 0.63 bar (see Figure S7). This increase indicates that the addition of nanofibers caused a significant increase in permeance, which may be related to several factors associated to the structure of the composite membrane, such as the tortuosity created by the nanofiber mesh. It can also be associated with increased hydrophilicity, as could be the case with the CL nanofibers. At a TMP of 3.5 bar, the CLNF-UF membranes had an observed flow rate of 697 m^3/s. These fluid

https://doi.org/10.1021/acs.iecr.1c01332
Ind. Eng. Chem. Res. XXXX, XXX, XXX−XXX

dynamic conditions result in a Reynolds number of 4.91×10^{-3} (basic calculations available by request), confirming that we are in the laminar regime. Based on our pure water flux values, it is possible that the nanofibers are creating a locally increased velocity of $\sim 6 \times 10^{-4}$ m/s, while the bulk fluid velocity is $\sim 4 \times 10^{-4}$ m/s.

Dead-End Pure Water Flux of Hydrophilic NF-UF100 Membranes. To directly compare the effect of hydrophobic to hydrophilic nanofibers, we surface-functionalized the PSf nanofibers with polydopamine to create crosslinked hydrophilic nanofibers.[30] This eliminated the shortcomings of the hydrophilic CL nanofibers, which swelled/were not crosslinked and had lower strength than the PSf. The average diameter of the hydrophilic-modified nanofibers remained statistically equivalent to the hydrophobic PSf nanofibers (1.0 μm), while their water contact angle dramatically decreased from 112 ± 5° to 36.5 ± 6.2°. Figure 6 demonstrates that the

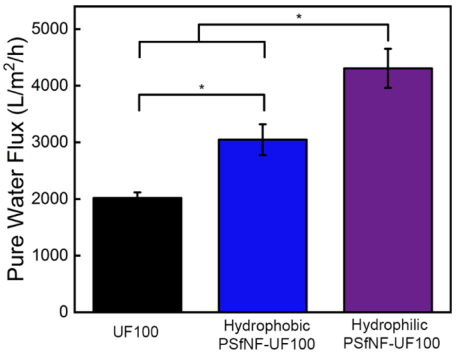

Figure 6. Dead-end pure water flux of hydrophobic- and hydrophilic-modified PSfNF-UF100 membranes. All nanofiber layers were 50 μm thick and tests were conducted at a TMP of 2 bar. Millipore membranes were used as the base. The error bars indicate standard deviation, and one asterisk (*) denotes $p < 0.05$ significance.

hydrophilic-modified NF-UF100 membranes had a statistically higher pure water flux than the hydrophobic PSfNF-UF100 and control membranes. These results again suggest that having an intact crosslinked fiber layer plays a significant role in improving membrane flux and that a crosslinked hydrophilic nanofiber layer is the best. This further supports our hypothesis as to why the CL did not outperform the PSf fibers.

Dead-End Oil Flux of CLNF-UF and PSfNF-UF Membranes. Next, we conducted dead-end flux experiments (at TMPs of 2.0 and 3.5 bar) using silicone oil, a hydrophobic liquid (Figure 7). The hydrophobic silicone oil was selected because it has similar fluid properties to water. The silicone oil has a viscosity of 0.98 cP and a specific gravity of 0.82, whereas water has a viscosity of 1 cP and a specific gravity of 1. The oil flux of the PSfNF-UF100 membranes was statistically greater than the controls at both TMPs, which was analogous to the results of the water flux experiments. It is interesting to note that the silicone oil flux of the CLNF-UF100 membranes at 3.5 bar was statistically equivalent to the control membranes; this contrasts the results in Figure 4, in which the pure water flux of the CLNF-UF100 membranes was lower than the control. This suggests that, indeed, the swelling of the CL fibers is causing a disadvantageous morphology when used with aqueous solutions. At 3.5 bar, the hydrophobic oil flux of the PSfNF-UF100 membranes increased by 65%, while the hydrophilic water flux increased by 30%. Potentially, by reducing the

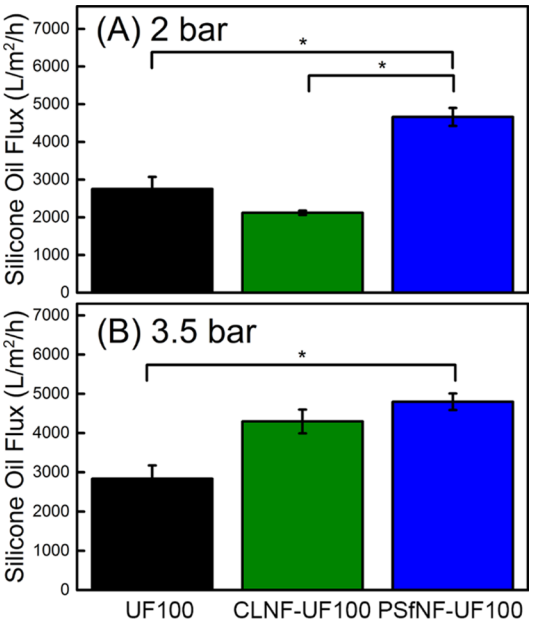

Figure 7. Dead-end oil flux of PSfNF- and CLNF-UF100 membranes at TMPs of (A) 2 bar and (B) 3.5 bar. All nanofiber layers were 50 μm thick. Synder membranes were used as the base. An operating pressure of 2 bar was used. The error bars indicate standard deviation, and one asterisk (*) denotes $p < 0.05$ significance.

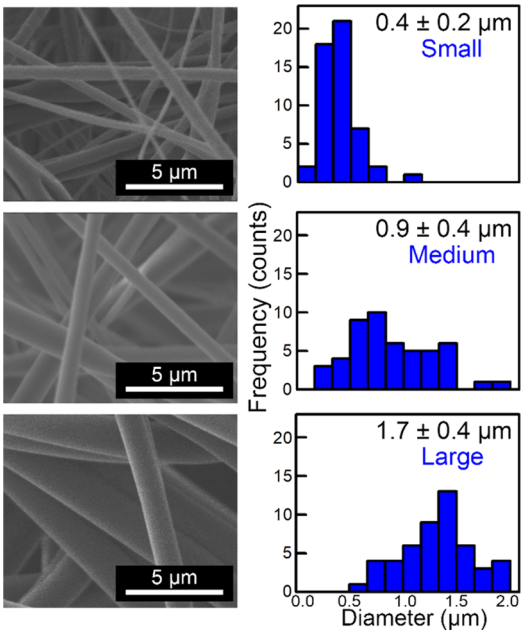

Figure 8. SEM micrographs of PSf nanofibers alongside their average fiber diameter and diameter distribution. The small, medium, and large PSf nanofibers were statistically different in average diameter from one another.

repulsion between the nanofiber surfaces and fluid (implicating a slip boundary condition),[54] we have increased the flux.

Pure Water Flux of PSfNF-UF200 as a Function of Individual Nanofiber Diameter. While the previous sections focused on altering the chemistry/hydrophilicity of the nanofiber layer and the feed solution, here, we focused on understanding how changing the surface area within the nanofiber layer impacted the flux. To do this, we fabricated PSf nanofibers with statistically different average diameters (Figure

https://doi.org/10.1021/acs.iecr.1c01332
Ind. Eng. Chem. Res. XXXX, XXX, XXX−XXX

8) by changing the electrospinning precursor solution. All fibers had a smooth and cylindrical morphology and three statistically different diameters, 0.4 ± 0.2, 0.9 ± 0.4, and 1.7 ± 0.4 μm, which will be referred to as small, medium, and large PSf nanofibers, respectively.

Figure 9 displays the pure water flux of PSfNF-UF200 membranes enhanced with small, medium, or large PSf nanofibers. In these experiments, the overall bulk thickness of the layer was held constant at 50 μm. The PSfNF-UF200 membranes with the smallest diameter fibers (0.4 μm) exhibited the greatest flux, which was statistically greater than the control and the medium PSfNF-UF200 membranes. The smallest diameter PSfNF-UF200 membranes that had the highest flux also had the greatest surface-to-area volume ratio. This supports our hypothesis that a high level of surface interactions might be key to increasing the flux as opposed to confinement effects, which are reported to occur in frictionless nanoscale carbon nanotubes.[55]

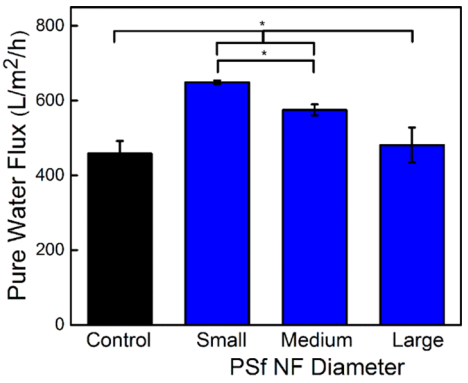

Figure 9. Dead-end flux of PSfNF-UF200 membranes a function of average fiber diameter. All nanofiber layers were 50 μm thick. Synder membranes were used as the base. An operating pressure of 2 bar was used. The error bars indicate standard deviation, and one asterisk (*) denotes $p < 0.05$ significance.

CONCLUSIONS

In this study, for the first time, we have systematically probed how membranes functionalized using well-characterized electrospun nanofibers impact the flux performance of ultrafiltration membranes. All base membranes (UF10, UF100, and UF200) exhibited a statistically greater pure water flux than the controls (no nanofibers) in the presence of a PSf nanofiber layer in both cross-flow and dead-end configurations. We found that the PSfNF-UF10 membranes, which had the smallest pore diameter and coverage, exhibited the largest increase in normalized flux, a 50% increase, whereas the PSfNF-UF100 and PSfNF-UF200 membranes exhibited an 11% and 14% improvement. The flux of the hydrophobic oil through the PSfNF-UF100 membranes was also statistically greater than the controls. By modulating the diameters of the individual fibers, our best results were obtained when crosslinked 50 μm-thick nanofibers layers were used with the smallest average diameter (400 nm) fiber because they had the highest internal surface area. Previously, it has been suggested that the velocity profile and magnitude of the velocity are greater when nanometer-scale spacers are composed of more "random" filaments with varying z-distances rather than a traditional cavity spacer[56] and it is possible that our nanofiber layers are acting as turbulence-inducing spacers. While, generally, PSf nanofibers outperformed the non-crosslinked CL nanofibers, by surface-functionalizing PSf fibers with a hydrophilic polydopamine layer, we achieved further increases in pure water flux over the crosslinked hydrophobic PSf nanofiber-enhanced membranes. Notably, in terms of durability, our composite membranes were robust; the nanofibers indicated no signs of failure or breakages even when testing was conducted at a TMP of 3.5 bar, which was the practical operation limit of our system. While this experimental work systematically probed the chemistry−structure−property relationships that govern nanofiber-enhanced membrane performance, future work should test the propensity of the nanofiber layers to foul. Notably, pathways toward fabricating highly antifouling nanofiber mats have previously been published.[30]

Here, we have demonstrated that adding a nanofiber layer to an ultrafiltration membrane offers a rational approach to functionalizing a membrane and improving flux performance. The greatest increase in flux performance arises from the smallest diameter hydrophilic nanofibers that are also highly crosslinked and mechanically robust. We suggest that making this layer of fine nanofibers via electrospinning is desirable because scalable manufacturing processes exist and the interconnected nature of the fibers alleviates concerns about their transport into the environment, which might be present from discontinuous nanofibers (i.e., carbon nanofibers).

ASSOCIATED CONTENT

Supporting Information

The Supporting Information is available free of charge at https://pubs.acs.org/doi/10.1021/acs.iecr.1c01332.

Compaction curves, FTIR spectra, cross-flow pure water flux, spacer coverage, and dead-end pure water flux (PDF)

AUTHOR INFORMATION

Corresponding Author

Jessica D. Schiffman − *Department of Chemical Engineering, University of Massachusetts Amherst, Amherst, Massachusetts 01003-9303, United States;* orcid.org/0000-0002-1265-5392; Email: schiffman@ecs.umass.edu

Authors

Kerianne M. Dobosz − *Department of Chemical Engineering, University of Massachusetts Amherst, Amherst, Massachusetts 01003-9303, United States;* orcid.org/0000-0003-4042-5399

Christopher A. Kuo-Leblanc − *Department of Chemical Engineering, University of Massachusetts Amherst, Amherst, Massachusetts 01003-9303, United States;* orcid.org/0000-0003-1112-2436

Jared W. Bowden − *Department of Chemical Engineering, University of Massachusetts Amherst, Amherst, Massachusetts 01003-9303, United States*

Complete contact information is available at: https://pubs.acs.org/10.1021/acs.iecr.1c01332

Notes

The authors declare no competing financial interest.

https://doi.org/10.1021/acs.iecr.1c01332
Ind. Eng. Chem. Res. XXXX, XXX, XXX−XXX

■ ACKNOWLEDGMENTS

We thank Dr. Alexander Ribbe, Dr. Michael Jercinovic, and Mr. Lou Raboin for their experimental guidance. This work was supported in part by a Fellowship from the University of Massachusetts to K.M.D. as part of the Biotechnology Training Program (National Research Service Award T32 GM108556). C.A.K.-L. and J.W.B. thank the Commonwealth Honors College for support. The authors acknowledge the support of the National Science Foundation (NSF 1342343 and 1719747).

■ REFERENCES

(1) Liu, L.; Johnson, H. L.; Cousens, S.; Perin, J.; Scott, S.; Lawn, J. E.; Rudan, I.; Campbell, H.; Cibulskis, R.; Li, M. Global, Regional, and National Causes of Child Mortality: An Updated Systematic Analysis for 2010 with Time Trends since 2000. *Lancet* **2012**, *379*, 2151.

(2) Victora, C. G.; Wagstaff, A.; Schellenberg, J. A.; Gwatkin, D.; Claeson, M.; Habicht, J.-P. Applying an Equity Lens to Child Health and Mortality: More of the Same Is Not Enough. *Lancet* **2003**, *362*, 233.

(3) Murray, P. R.; Rosenthal, K. S.; Pfaller, M. A. *Medical Microbiology*; Elsevier Mosby: Philadelphia, 2005.

(4) Owoseni, M.; Olaniran, A.; Okoh, A. Chlorine Tolerance and Inactivation of *Escherichia coli* Recovered from Wastewater Treatment Plants in the Eastern Cape. *South Africa. Appl. Sci.* **2017**, *7*, 810.

(5) G.K., Dhawan. *Back To Basics: About Ultrafiltration (UF)*. https://www.appliedmembranes.com/back-to-basics-about-ultrafiltration-uf.html.

(6) Dobosz, K. M.; Kolewe, K. W.; Schiffman, J. D. Green Materials Science and Engineering Reduces Biofouling: Approaches for Medical and Membrane-Based Technologies. *Front. Microbiol.* **2015**, *6*, 196.

(7) Zhang, R.; Liu, Y.; He, M.; Su, Y.; Zhao, X.; Elimelech, M.; Jiang, Z. Antifouling Membranes for Sustainable Water Purification: Strategies and Mechanisms. *Chem. Soc. Rev.* **2016**, *45*, 5888.

(8) Dobosz, K. M.; Kuo-LeBlanc, C. A.; Emrick, T.; Schiffman, J. D. Antifouling Ultrafiltration Membranes with Retained Pore Size by Controlled Deposition of Zwitterionic Polymers and Poly(Ethylene Glycol). *Langmuir* **2019**, *35*, 1872.

(9) Heinz, O.; Aghajani, M.; Greenberg, A. R.; Ding, Y. Surface-Patterning of Polymeric Membranes: Fabrication and Performance. *Curr. Opin. Chem. Eng.* **2018**, *20*, 1.

(10) Remanan, S.; Sharma, M.; Bose, S.; Das, N. C. Recent Advances in Preparation of Porous Polymeric Membranes by Unique Techniques and Mitigation of Fouling through Surface Modification. *ChemistrySelect* **2018**, *3*, 609.

(11) Maruf, S. H.; Li, Z.; Yoshimura, J. A.; Xiao, J.; Greenberg, A. R.; Ding, Y. Influence of Nanoimprint Lithography on Membrane Structure and Performance. *Polymer* **2015**, *69*, 129.

(12) Maruf, S. H.; Greenberg, A. R.; Pellegrino, J.; Ding, Y. Fabrication and Characterization of a Surface-Patterned Thin Film Composite Membrane. *J. Memb. Sci.* **2014**, *452*, 11.

(13) Maruf, S. H.; Wang, L.; Greenberg, A. R.; Pellegrino, J.; Ding, Y. Use of Nanoimprinted Surface Patterns to Mitigate Colloidal Deposition on Ultrafiltration Membranes. *J. Memb. Sci.* **2013**, *428*, 598.

(14) He, X.; Wang, T.; Li, Y.; Chen, J.; Li, J. Fabrication and Characterization of Micro-Patterned PDMS Composite Membranes for Enhanced Ethanol Recovery. *J. Memb. Sci.* **2018**, *563*, 447.

(15) Won, Y.-J.; Choi, D.-C.; Jang, J. H.; Lee, J.-W.; Chae, H. R.; Kim, I.; Ahn, K. H.; Lee, C.-H.; Kim, I.-C. Factors Affecting Pattern Fidelity and Performance of a Patterned Membrane. *J. Memb. Sci.* **2014**, *462*, 1.

(16) Choi, D.-C.; Jung, S.-Y.; Won, Y.-J.; Jang, J. H.; Lee, J.-W.; Chae, H.-R.; Lim, J.; Ahn, K. H.; Lee, S.; Kim, J.-H.; Park, P.-K.; Lee, C.-H. Effect of Pattern Shape on the Initial Deposition of Particles in the Aqueous Phase on Patterned Membranes during Crossflow Filtration. *Environ. Sci. Technol. Lett.* **2017**, *4*, 66.

(17) Weinman, S. T.; Fierce, E. M.; Husson, S. M. Nanopatterning Commercial Nanofiltration and Reverse Osmosis Membranes. *Sep. Purif. Technol.* **2019**, *209*, 646.

(18) ElSherbiny, I. M. A.; Khalil, A. S. G.; Ulbricht, M. Surface Micro-Patterning as a Promising Platform towards Novel Polyamide Thin-Film Composite Membranes of Superior Performance. *J. Memb. Sci.* **2017**, *529*, 11.

(19) Liu, T.; Zhou, H.; Graham, N.; Lian, Y.; Yu, W.; Sun, K. The Antifouling Performance of an Ultrafiltration Membrane with Pre-Deposited Carbon Nanofiber Layers for Water Treatment. *J. Memb. Sci.* **2018**, *557*, 87.

(20) Dobosz, K. M.; Kuo-Leblanc, C. A.; Martin, T. J.; Schiffman, J. D. Ultrafiltration Membranes Enhanced with Electrospun Nanofibers Exhibit Improved Flux and Fouling Resistance. *Ind. Eng. Chem. Res.* **2017**, *56*, 5724.

(21) Díez, B.; Amariei, G.; Rosal, R. Electrospun Composite Membranes for Fouling and Biofouling Control. *Ind. Eng. Chem. Res.* **2018**, *57*, 14561.

(22) Ghasemi-Mobarakeh, L.; Semnani, D.; Morshed, M. A Novel Method for Porosity Measurement of Various Surface Layers of Nanofibers Mat Using Image Analysis for Tissue Engineering Applications. *J. Appl. Polym. Sci.* **2007**, *106*, 2536.

(23) Persano, L.; Camposeo, A.; Tekmen, C.; Pisignano, D. Industrial Upscaling of Electrospinning and Applications of Polymer Nanofibers: A Review. *Macromol. Mater. Eng.* **2013**, *298*, 504.

(24) Wu, Z.; Chen, Z.; Du, X.; Logan, J. M.; Sippel, J.; Nikolou, M.; Kamaras, K.; Reynolds, J. R.; Tanner, D. B.; Hebard, A. F.; Rinzler, A. G. Transparent, Conductive Carbon Nanotube Films. *Science* **2004**, *305*, 1273.

(25) Ma, H.; Hsiao, B. S. Current Advances on Nanofiber Membranes for Water Purification Applications. In *Filtering Media by Electrospinning: Next Generation Membranes for Separation Applications*; Springer: New York, 2018.

(26) Ahmed, F. E.; Lalia, B. S.; Hashaikeh, R. A Review on Electrospinning for Membrane Fabrication: Challenges and Applications. *Desal. Elsevier* **2015**, *356*, 15.

(27) Waisi, B. I.; Manickam, S. S.; Benes, N. E.; Nijmeijer, A.; McCutcheon, J. R. Activated Carbon Nanofiber Nonwovens: Improving Strength and Surface Area by Tuning Fabrication Procedure. *Ind. Eng. Chem. Res.* **2019**, *58*, 4084.

(28) Feroz, H.; Bai, M.; Kwon, H.; Brezovec, J.; Peng, J.; Kumar, M. Can Fibrous Mats Outperform Current Ultrafiltration and Microfiltration Membranes? *Ind. Eng. Chem. Res.* **2017**, *56*, 10438.

(29) Ma, Z.; Ramakrishna, S. Electrospun Regenerated Cellulose Nanofiber Affinity Membrane Functionalized with Protein A/G for IgG Purification. *J. Memb. Sci.* **2008**, *319*, 23.

(30) Kolewe, K. W.; Dobosz, K. M.; Rieger, K. A.; Chang, C.-C.; Emrick, T.; Schiffman, J. D. Antifouling Electrospun Nanofiber Mats Functionalized with Polymer Zwitterions. *ACS Appl. Mater. Interfaces* **2016**, *8*, 27585.

(31) Şenbil, N.; He, W.; Démery, V.; Dinsmore, A. D.; Senbil, N.; He, W.; Démery, V.; Dinsmore, A. D. Effect of Interface Shape on Advancing and Receding Fluid-Contact Angles around Spherical Particles. *Soft Matter* **2015**, *11*, 4999.

(32) Yip, N. Y.; Tiraferri, A.; Phillip, W. A.; Schiffman, J. D.; Elimelech, M. High Performance Thin-Film Composite Forward Osmosis Membrane. *Environ. Sci. Technol.* **2010**, *44*, 3812.

(33) Schneider, C. A.; Rasband, W. S.; Eliceiri, K. W. NIH Image to ImageJ: 25 Years of Image Analysis. *Nat. Methods* **2012**, *9*, 671.

(34) Ali, N.; Tari, S. S. M. Surface Modification of Polyethersulfone Ultrafiltration (PES-UF) Membrane Using Myoglobin as Modifying Agent. *Desalin. Water Treat.* **2012**, *47*, 171.

(35) Taurozzi, J. S.; Arul, H.; Bosak, V. Z.; Burban, A. F.; Voice, T. C.; Bruening, M. L.; Tarabara, V. V. Effect of Filler Incorporation Route on the Properties of Polysulfone−Silver Nanocomposite Membranes of Different Porosities. *J. Memb. Sci.* **2008**, *325*, 58.

https://doi.org/10.1021/acs.iecr.1c01332
Ind. Eng. Chem. Res. XXXX, XXX, XXX−XXX

(36) Luo, C. J.; Stoyanov, S. D.; Stride, E.; Pelan, E.; Edirisinghe, M. Electrospinning versus Fibre Production Methods: From Specifics to Technological Convergence. *Chem. Soc. Rev.* **2012**, *41*, 4708.
(37) Kasemset, S.; He, Z.; Miller, D. J.; Freeman, B. D.; Sharma, M. M. Effect of Polydopamine Deposition Conditions on Polysulfone Ultrafiltration Membrane Properties and Threshold Flux during Oil/Water Emulsion Filtration. *Polymer* **2016**, *97*, 247.
(38) Feng, C.; Khulbe, K. C.; Matsuura, T.; Tabe, S.; Ismail, A. F. Preparation and Characterization of Electro-Spun Nanofiber Membranes and Their Possible Applications in Water Treatment. *Sep. Purif. Technol.* **2013**, *102*, 118.
(39) Homaeigohar, S. S.; Buhr, K.; Ebert, K. Polyethersulfone Electrospun Nanofibrous Composite Membrane for Liquid Filtration. *J. Memb. Sci.* **2010**, *365*, 68.
(40) Rieger, K. A.; Thyagarajan, R.; Hoen, M. E.; Yeung, H. F.; Ford, D. M.; Schiffman, J. D. Transport of Microorganisms into Cellulose Nanofiber Mats. *Langmuir* **2016**, *6*, 24438.
(41) Jonoobi, M.; Harun, J.; Mathew, A. P.; Hussein, M. Z. B.; Oksman, K. Preparation of Cellulose Nanofibers with Hydrophobic Surface Characteristics. *Cellulose* **2009**, *17*, 299.
(42) Bormashenko, E.; Pogreb, R.; Whyman, G.; Bormashenko, Y.; Jager, R.; Stein, T.; Schechter, A.; Aurbach, D. The Reversible Giant Change in the Contact Angle on the Polysulfone and Polyethersulfone Films Exposed to UV Irradiation. *Langmuir* **2008**, *24*, 5977.
(43) Gopal, R.; Kaur, S.; Feng, C. Y.; Chan, C.; Ramakrishna, S.; Tabe, S.; Matsuura, T. Electrospun Nanofibrous Polysulfone Membranes as Pre-Filters: Particulate Removal. *J. Memb. Sci.* **2007**, *289*, 210.
(44) *Biomax Membranes: The Membrane of Choice for Fast Processing and Exceptional Chemical Resistance*; EMD Millipore: Billerica, MA, 2015.
(45) Hoover, L. A.; Schiffman, J. D.; Elimelech, M. Nanofibers in Thin-Film Composite Membrane Support Layers: Enabling Expanded Application of Forward and Pressure Retarded Osmosis. *Desalination* **2013**, *308*, 73.
(46) Qing, Y.; Wu, Y.; Cai, Z.; Li, X. Water-Triggered Dimensional Swelling of Cellulose Nanofibril Films: Instant Observation Using Optical Microscope. *J. Nanomater.* **2013**, *2013*, 1.
(47) Gindl, W.; Martinschitz, K. J.; Boesecke, P.; Keckes, J. Changes in the Molecular Orientation and Tensile Properties of Uniaxially Drawn Cellulose Films. *Biomacromolecules* **2006**, *7*, 3146.
(48) Miyake, H.; Gotoh, Y.; Ohkoshi, Y.; Nagura, M. Tensile Properties of Wet Cellulose. *Polym. J.* **2000**, *32*, 29.
(49) Eichhorn, S. J.; Sampson, W. W. Relationships between Specific Surface Area and Pore Size in Electrospun Polymer Fibre Networks. *J. R. Soc., Interface* **2010**, *7*, 641.
(50) Shou, D.; Fan, J.; Ding, F. Hydraulic Permeability of Fibrous Porous Media. *Int. J. Heat Mass Transfer* **2011**, *54*, 4009.
(51) El, O. A.; Ae, S.; Fidale, L. C.; Naiara, A. E.; Ae, R.; Luiza, M.; Ae, A.; Frollini, E.; Ruiz, N.; Química, N.; Paulo, S.; D'almeida, B. M. L. O.; Frollini, B. E. Cellulose Swelling by Protic Solvents: Which Properties of the Biopolymer and the Solvent Matter? *Cellulose* **2008**, *15*, 371.
(52) Dods, S. R.; Hardick, O.; Stevens, B.; Bracewell, D. G. Fabricating Electrospun Cellulose Nanofibre Adsorbents for Ion-Exchange Chromatography. *J. Chromatogr. A* **2015**, *1376*, 74.
(53) Liu, L.; Pan, Z. Properties of Hydrophilic Chitosan / Polysulfone Nanofibrous Filtration Membrane. *J. Eng. Fiber. Fabr.* **2014**, *9*, 76.
(54) Priezjev, N. V.; Darhuber, A. A.; Troian, S. M. Slip Behavior in Liquid Films on Surfaces of Patterned Wettability: Comparison between Continuum and Molecular Dynamics Simulations. *Phys. Rev. E* **2005**, *71*, No. 041608.
(55) Majumder, M.; Chopra, N.; Andrews, R.; Hinds, B. J. Enhanced Flow in Carbon Nanotubes. *Nature* **2005**, *438*, 44.
(56) Ma, S.; Song, L. Numerical Study on Permeate Flux Enhancement by Spacers in a Crossflow Reverse Osmosis Channel. *J. Memb. Sci.* **2006**, *284*, 102.

https://doi.org/10.1021/acs.iecr.1c01332
Ind. Eng. Chem. Res. XXXX, XXX, XXX−XXX